Acta Mechanica 181, 1–17 (2006)
DOI 10.1007/s00707-005-0279-2

Acta Mechanica
Printed in Austria

Elastoplastic modeling of progressive interfacial debonding for particle-reinforced metal-matrix composites

H. T. Liu, L. Z. Sun, Iowa City, Iowa, and **J. W. Ju,** Los Angeles, California

Received March 10, 2005; revised June 30, 2005
Published online: November 7, 2005 © Springer-Verlag 2005

Summary. The purpose of this study is to model the elastoplastic behavior of particle-reinforced metal-matrix composites with particle-matrix interfacial debonding. The partially debonding process at the interface is represented by the debonding angles. The equivalent orthotropic elastic moduli are constructed for the debonded yet isotropic particles to characterize the reduction of the load-transfer ability in the debonded directions. To simulate the debonding evolution and the transition between various debonding modes, the volume fractions of various particles are expressed in terms of the Weibull's statistical functions. Micromechanical homogenization procedures are utilized to estimate the effective moduli and the overall yield function of the resultant multi-phase composites. The associative plastic flow rule and isotropic hardening law are postulated based on the continuum plasticity theory. The effects of partially interfacial debonding on the overall yield surfaces and stress-strain relations of the composites are investigated and illustrated via numerical examples as well.

1 Introduction

In the last few decades, particle-reinforced metal-matrix composites (PRMMCs) have been rapidly developed to meet the need for better materials with higher standards of performance and in-service reliability. While the enhanced mechanical properties mostly come from the reinforcing particle phase, the latter also leads to new damage mechanisms that restrict the potential for widespread use of composites. Minimizing these limitations through microstructural design requires a thorough understanding of the micro-mechanisms of their intrinsic damage processes. Among the three prevalent damage micro-mechanisms in PRMMCs (i.e., debonding at the matrix-particle interface, internal particle-cracking, and ductile plastic localization in the matrix [1], [2]), matrix-particle interfacial debonding is the predominant damage mode when the interfacial strength is relatively weak and the composite system is under high triaxial loading. To model the interfacial debonding in composites, Jasiuk and Tong [3], Pagano and Tandon [4], Qu [5], Sangani and Mo [6] introduced either a linear spring-layer with vanishing thickness or an inter-layer with constant thickness. In their models, a different elastic constant of the spring-/inter-layer from the matrix and reinforcements is used to simulate the loss of load-transfer ability through the interface due to debonding. Since the spring-/inter-layer elastic properties in their models are not position-dependent, their models are not applicable for

partial debonding mechanisms. Another simple yet physically meaningful means used to model the interfacial debonding is the equivalent stiffness method [7]–[9] in which the isotropic debonded particles are replaced by the perfectly bonded particles with constructed equivalent anisotropic stiffness to characterize the reduction of the load-transfer ability of the debonded interface. Thus, the conventional Eshelby's inclusion theory and the micromechanics method [10]–[12] can be applied to deal with the multi-phase composites.

To capture the progressive process of the interfacial debonding, the evolution of the damage, and the transition between various debonding modes, the present authors have recently developed a micromechanical framework to simulate the interfacial debonding between the matrix and reinforcing particles, and to estimate its effect on the overall *elastic* behavior of particle-reinforced composites [13]. In this model, the progressive damage process is represented by the debonding angles that are governed by external loads. To extend the study, a *plastic* model is proposed in this paper to investigate the effect of the progressive partial interfacial-debonding on the overall nonlinear response of ductile composites containing randomly dispersed particles. The effective yield function of the composite with partial interfacial debonding is derived in explicit form, and the effective elastoplastic-damage constitutive behaviors of the composites under various loading conditions are numerically simulated and compared with available experimental results.

2 Progressive interfacial debonding model

In this study, the ductile composites with randomly distributed spherical particles are considered. With the increase of the applied loads, some particles may start to debond from the matrix; see Fig. 1. To model the progressive interfacial debonding, the micromechanical model proposed by Liu et al. [13] is adopted in this study and briefly reviewed in this section.

2.1 Debonding modes

Interfacial debonding is a local phenomenon. Emanating from the assumption that the normal stress controls the debonding initiation on the interface, as the (tensile) normal stress reaches a critical interfacial bonding strength σ_{cri}, the debonding process would initiate at the point P. The debonding criterion can be conveniently written as

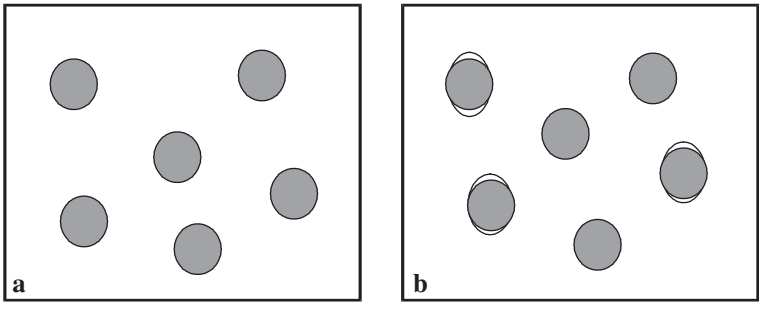

Fig. 1. Schematic diagram of microstructures of PRMMCs: **a** Initial state (undamaged); **b** interfacial debonding under loading

$$\sigma^{\text{normal}} = \sigma_{\text{cri}}. \tag{1}$$

Here, the local normal stress σ^{normal} can be expressed as the three local principal stresses ($\sigma_1, \sigma_2, \sigma_3$ and $\sigma_1 \geq \sigma_2 \geq \sigma_3$) under the local Cartesian coordinate system as

$$\sigma^{\text{normal}} = \sigma_1(\sin\phi\cos\theta)^2 + \sigma_2(\sin\phi\sin\theta)^2 + \sigma_3(\cos\phi)^2, \tag{2}$$

where the three axes of the local coordinates coincide with the three principal directions of the local stress field $\boldsymbol{\sigma}$ inside a particle. θ and ϕ are the two Eulerian angles shown in Fig. 2. The local stress field $\boldsymbol{\sigma}$ inside a particle can be calculated using Eshelby's micromechanical theory [10], [11] and the equivalent method that is described in [13].

The relationship between the local principal stresses and the critical debonding strength results in the following four different types of interfacial debonding modes. Here, the debonding area is represented using two debonding angles that are defined corresponding to various debonding modes (see Fig. 3). In mode 1 ($\sigma_{\text{cri}} \geq \sigma_1 \geq \sigma_2 \geq \sigma_3$), the particle is perfectly bonded to the matrix since none of the principal stresses reaches the critical bonding strength. In mode 2 ($\sigma_1 \geq \sigma_{\text{cri}} \geq \sigma_2 \geq \sigma_3$), only one principal stress is greater than the critical interfacial bonding strength σ_{cri}. Therefore, the interfacial debonding initiates from the local x_1-direction and propagates progressively towards the other two principal directions. The debonding area (the shaded area in Fig. 3a) is represented by the corresponding debonding angles $\alpha_{12}^{(2)}$ and $\alpha_{13}^{(2)}$ (cf. Fig. 3a), which can be calculated based on the debonding criterion Eq. (1) and the normal stress expression Eq. (2) as

$$\alpha_{1\gamma}^{(2)} = \sin^{-1}\sqrt{\frac{\sigma_1 - \sigma_{\text{cri}}}{\sigma_1 - \sigma_\gamma}}, \quad \gamma = 2, 3. \tag{3}$$

When $\sigma_1 \geq \sigma_2 \geq \sigma_{\text{cri}} > \sigma_3$, mode 3 debonding is activated. The debonding is complete in the entire x_1–x_2 plane and develops from the x_1- and x_2-axes towards the x_3-axis, respectively. The two corresponding debonding angles $\alpha_{13}^{(3)}$ and $\alpha_{23}^{(3)}$ (Fig. 3b) denote the debonding processes in the planes of x_1–x_3 and x_2–x_3, respectively, and can be expressed as follows:

$$\alpha_{\gamma 3}^{(3)} = \sin^{-1}\sqrt{\frac{\sigma_\gamma - \sigma_{\text{cri}}}{\sigma_\gamma - \sigma_3}}, \quad \gamma = 1, 2. \tag{4}$$

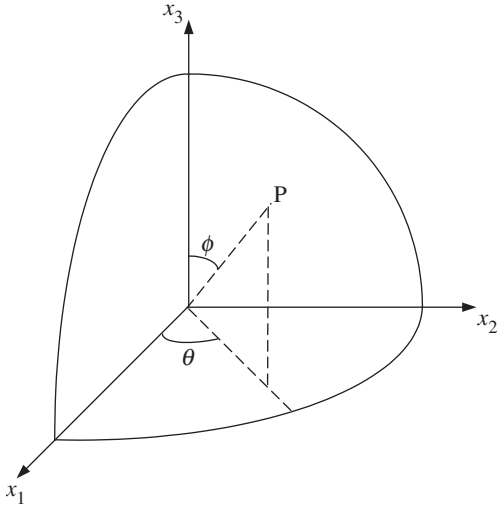

Fig. 2. Two Eulerian angles θ and ϕ representing the surface point P on the one-eighth of spherical particle in the local coordinates

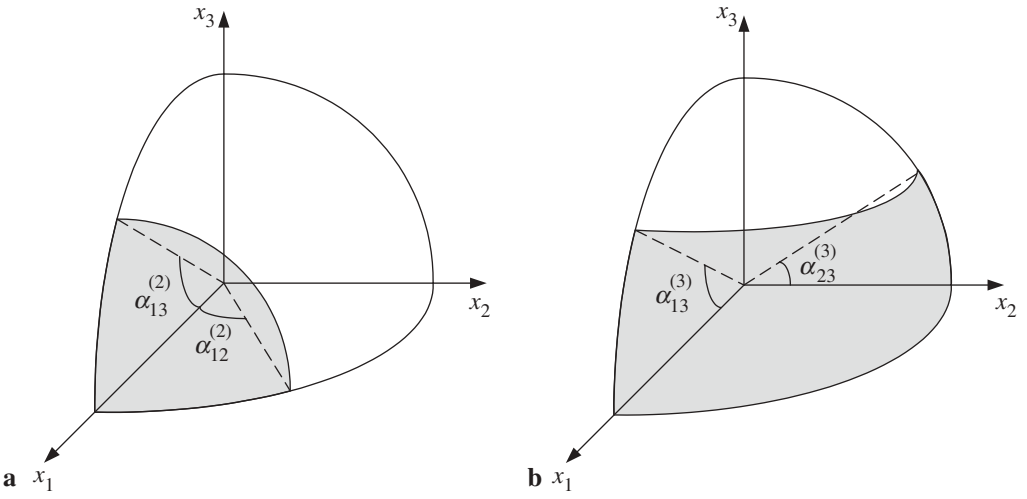

Fig. 3. The debonding areas and debonding angles of **a** mode 2, and **b** mode 3 interfacial debonding

Finally, in mode 4, when all three principal stresses exceed the critical bonding strength, the normal stress at any point on a particle surface is greater than the critical strength. The entire interface is now debonded. It is noted that, for all of the above four different debonding modes, the range of debonding angles is between 0 and $\pi/2$. The lower and upper bounds of the debonding angles in a certain pair of principal directions correspond to the perfect bonding and total debonding, respectively, between these directions.

2.2 Equivalent elastic stiffness for debonded particles

The partially interfacial debonding results in the *partial* loss of load-transfer capacity in the debonding directions, which is simulated by the reduction of the corresponding elastic stiffness of the debonded particles in that direction [13], [14]. Therefore, the partially debonded isotropic particles are replaced by perfectly bonded particles with constructed equivalent orthotropic stiffness tensors. To establish the relationship between the debonding angles and the loss of tensile load-transfer capacity, which is manifested by a reduction in elastic stiffness, three distinct interfacial damage parameters $D_i^{(\beta)}$ serving as the measures of elastic stiffness reduction in certain directions are defined using the ratio between the projected damage area in a certain direction and the original interface area. Here, the superscript $\beta = 1, 2, 3, 4$ refers to the four distinct debonding modes and the subscript $i = 1, 2, 3$ represents the damage effect on the three principal directions, respectively. For instance, Fig. 4 shows an example of mode 2 debonding, where the debonding parameters are defined as $D_1^{(2)} \triangleq A_1/A$, $D_2^{(2)} \triangleq A_2/A$ and $D_3^{(2)} \triangleq A_3/A$, respectively.

In accordance with the four different debonding modes presented in the previous section, the interfacial damage parameters can be developed as follows for various debonding modes, respectively:

$$D_1^{(1)} = D_2^{(1)} = D_3^{(1)} = 0, \tag{5}$$

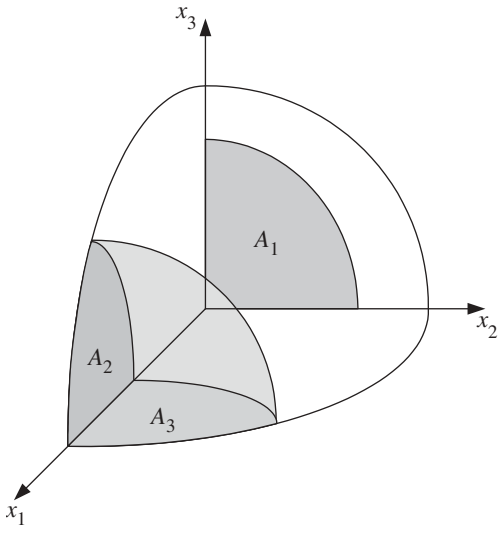

Fig. 4. The damage parameters are defined as the ratio between the projected damaged area in a certain direction and the original interface area interfacial debonding

$$D_1^{(2)} = \sin\alpha_{12}^{(2)} \sin\alpha_{13}^{(2)},$$

$$D_2^{(2)} \frac{2}{\pi}\left[\alpha_{13}^{(2)} - \frac{\sin\alpha_{13}^{(2)} \cos^2\alpha_{12}^{(2)} \sinh^{-1}\left(\sqrt{\sin^2\alpha_{12}^{(2)} - \sin^2\alpha_{13}^{(2)}}/\cos\alpha_{12}^{(2)}\right)}{\sqrt{\sin^2\alpha_{12}^{(2)} - \sin^2\alpha_{13}^{(2)}}}\right],$$

$$D_3^{(2)} = \frac{2}{\pi}\left[\alpha_{12}^{(2)} - \frac{\sin\alpha_{12}^{(2)} \cos^2\alpha_{13}^{(2)} \sin^{-1}\left(\sqrt{\sin^2\alpha_{12}^{(2)} - \sin^2\alpha_{13}^{(2)}}/\cos\alpha_{13}^{(2)}\right)}{\sqrt{\sin^2\alpha_{12}^{(2)} - \sin^2\alpha_{13}^{(2)}}}\right], \tag{6}$$

$$D_1^{(3)} = \frac{2}{\pi}\left[\alpha_{23}^{(3)} + \frac{\sin^2\alpha_{13}^{(3)} \cos\alpha_{23}^{(3)} \sin^{-1}\left(\sqrt{\sin^2\alpha_{13}^{(3)} - \sin^2\alpha_{23}^{(3)}}/\sin\alpha_{13}^{(3)}\right)}{\sqrt{\sin^2\alpha_{13}^{(3)} - \sin^2\alpha_{23}^{(3)}}}\right],$$

$$D_2^{(3)} = \frac{2}{\pi}\left[\alpha_{13}^{(3)} + \frac{\sin^2\alpha_{23}^{(3)} \cos\alpha_{13}^{(3)} \sinh^{-1}\left(\sqrt{\sin^2\alpha_{13}^{(3)} - \sin^2\alpha_{23}^{(3)}}/\sin\alpha_{23}^{(3)}\right)}{\sqrt{\sin^2\alpha_{13}^{(3)} - \sin^2\alpha_{23}^{(3)}}}\right], \tag{7}$$

$$D_3^{(3)} = 1 - \cos\alpha_{13}^{(3)} \cos\alpha_{23}^{(3)},$$

$$D_1^{(4)} = D_2^{(4)} = D_3^{(4)} = 1. \tag{8}$$

The debonding damage parameters vary from 0 to 1. A greater value of the damage parameter signifies a more significant level of *reduction* in tensile load-transfer capability.

With the help of the above damage parameters defined in Eqs. (5)–(8), the equivalent orthotropic stiffness tensors for the β-mode ($\beta = 1, 2, 3, 4$) partially debonded particles are constructed as follows to decrease the load-transfer ability of damaged particles:

$$C_{ijkl}^{(\beta)} = \lambda_{IK}^{(\beta)} \delta_{ij}\delta_{kl} + \mu_{IJ}^{(\beta)}(\delta_{ik}\delta_{jl} + \delta_{il}\delta_{jk}), \tag{9}$$

where

$$\begin{aligned}\lambda_{IK}^{(\beta)} &= \lambda^{(1)}\left(1-D_I^{(\beta)}\right)\left(1-D_K^{(\beta)}\right),\\ \mu_{IJ}^{(\beta)} &= \mu^{(1)}\left(1-D_I^{(\beta)}\right)\left(1-D_J^{(\beta)}\right),\end{aligned} \tag{10}$$

where $\lambda^{(1)}$ and $\mu^{(1)}$ denote the isotropic Lame constants of the original (perfectly bonded) particles and δ_{ij} is the Kronecker delta. Here, we follow Mura's tensorial indicial notation [12], i.e., the repeated lower-case indices are summed up from 1 to 3, whereas the upper-case indices take on the same numbers as the corresponding lower-case ones but are not summed up. This indicial expression facilitates the subsequent derivations and computations.

By using the elastic equivalency treatment, all partially debonded particles are replaced by perfectly bonded particles with the aforementioned equivalent orthotropic elastic stiffnesses. Therefore, multi-phase micromechanical approaches can be established to characterize the progressive interfacial debonding processes of metal matrix composites.

2.3 Microstructural damage evolution of particle debonding

The evolution of the volume fractions of the damaged particles can be simulated using a two-parameter Weibull distribution function as [15]

$$P_i = \begin{cases} 1-\exp\left[-\left(\frac{\sigma_i-\sigma_{\mathrm{cri}}}{S}\right)^M\right], & \sigma_i \geq \sigma_{\mathrm{cri}} \\ 0, & \sigma_i < \sigma_{\mathrm{cri}} \end{cases} \quad (i=1,2,3). \tag{11}$$

Here, the Weibull parameter M signifies the evolution rate of the volume fraction of debonded particles. The parameter S is not independent when the relationship between the mean value of the Weibull distribution function and the critical bonding strength σ_{cri} is established. For example, when an intermediate debonding evolution rate $M = 5$ is chosen and the mean of the Weibull function is equal to the critical bonding strength, S can be calculated as $S = 1.09\sigma_{\mathrm{cri}}$.

The volume fractions of the four various damage modes $\phi^{(\beta)}$ ($\beta = 1,2,3,4$) are expressed as follows to characterize the evolution of interfacial partial debonding and the transition between the four debonding modes:

$$\begin{aligned}\phi^{(4)} &= \phi^{\mathrm{Total}}P_3,\\ \phi^{(3)} &= \phi^{\mathrm{Total}}[P_2-P_3],\\ \phi^{(2)} &= \phi^{\mathrm{Total}}[P_1-P_2],\\ \phi^{(1)} &= \phi^{\mathrm{Total}}[1-P_1],\end{aligned} \tag{12}$$

where ϕ^{Total} is the total volume fraction of all particles in the composite. The probabilistic function P_i ($i = 1,\ 2,\ 3$) (Eq. (11)) represents a normal stress controlled debonding process and can be treated as the debonding probability in the i-th principal direction. When the smallest principal stress (the third principal stress) reaches the critical stress, the other two principal stresses are greater or equal to the critical stress, and thus the total debonding (the fourth mode) occurs. Therefore, the evolution of the fourth debonding mode is characterized by P_3. Similarly, the third debonding mode (two-dimensional debonding) and the second debonding mode (one-dimensional debonding) are controlled by P_2 and P_1, respectively. With the increase of external loading, part of the two-dimensional debonding converts to the total debonding, and part of the one-dimensional debonding evolves into the two-dimensional debonding.

Hence, the volume fractions of the four debonding modes are constructed as Eq. (12) to reflect the transition of debonding modes.

3 Effective yield function

Although the plastic deformation in composites is highly localized, the mean-field principles (homogenization procedures) can be directly applied to estimate the effective yield strength of composites since the initial yielding and plastic hardening of composites should be attributed to the collective responses of particle-matrix interactions [12]. To obtain the effective yield function of PRMMCs, the averaging homogenization is generally performed within a mesoscopic representative volume element (RVE); see, e.g., Nemat-Nasser and Hori [16]. At any local matrix material point $\mathbf{x}$, the microscopic stress $\boldsymbol{\sigma}(\mathbf{x})$ is assumed to satisfy the von Mises J_2-yield criterion and the local matrix yield function takes the form

$$F(\boldsymbol{\sigma}, \bar{e}_m^p) = \sqrt{\boldsymbol{\sigma} : \mathbf{I}_d : \boldsymbol{\sigma}} - K(\bar{e}_m^p) \leq 0, \tag{13}$$

where $\bar{e}_m^p$ and $K(\bar{e}_m^p)$ are the equivalent plastic strain and the isotropic hardening function of the matrix-only material, respectively. Moreover, $\mathbf{I}_d$ denotes the deviatoric part of the fourth-rank identity tensor $\mathbf{I}$.

Following the ensemble-volume averaging processes proposed by Ju and Sun [17], the overall yield function for the composites can be expressed as

$$\bar{F} = (1 - \phi^{(1)})\sqrt{\langle H \rangle_m} - K(\bar{e}^p) \leq 0, \tag{14}$$

where $\bar{e}^p$ represents the effective equivalent plastic strain. It should be noted that the effect of the various debonding modes on the overall yield function is reflected through the change of stress field. This is shown in the expression of $\langle H \rangle_m$, which is a function of the volume fraction $\phi^{(i)}$, $(i = 1, 2, 3, 4)$ (see Eqs. (19) and (20)). The expression of $\langle H \rangle_m$ for the composite with four phases of particles (corresponding to the four debonding modes) can be approximately obtained by neglecting the interaction among neighboring particles as

$$\langle H \rangle_m(x) \cong H^0 + \sum_{\beta=1}^{4} \oint_{\mathbf{x}' \notin \Xi(\mathbf{x})} [H^{(\beta)}(\mathbf{x}|\mathbf{x}') - H^0] P^{(\beta)}(\mathbf{x}')\, d\mathbf{x}', \tag{15}$$

where $H^0 = \boldsymbol{\sigma}_0 : \mathbf{I}_d : \boldsymbol{\sigma}_0$ is the square of the far-field stress norm applied on the composite and $\Xi(\mathbf{x})$ is the exclusion zone of $\mathbf{x}$ for the center location $\mathbf{x}'$ of a particle in the probability space, which is identical to the shape and size of the particle. $P^{(\beta)}(\mathbf{x}')$ is the probability density function for finding a β-phase particle in the exclusion zone of the particle center located at $\mathbf{x}'$. In addition, $H^{(\beta)}$ is the stress-norm collection contribution from the β-phase particles, i.e.,

$$H^{(\beta)} = \boldsymbol{\sigma}^{(\beta)}(\mathbf{x}) : \mathbf{I}_d : \boldsymbol{\sigma}^{(\beta)}(\mathbf{x}), \quad \beta = 1, 2, 3, 4, \tag{16}$$

where the local stress tensor in the matrix due to a β-phase particle centered at $\mathbf{x}'$ can be written as (cf. [17])

$$\boldsymbol{\sigma}(\mathbf{x}) = \boldsymbol{\sigma}_0 + \mathbf{C}^0 : \bar{\mathbf{G}}(\mathbf{x} - \mathbf{x}') : \boldsymbol{\epsilon}_*^{(\beta)}, \tag{17}$$

in which $\boldsymbol{\epsilon}_*^{(\beta)}$ is the eigenstrain tensor in the β-phase particles that can be expressed explicitly for spherical particles [13]; $\bar{\mathbf{G}}$ is the exterior-point Eshelby's tensor [18] and has the following simple form for spherical particles:

$$\bar{G}_{ijkl}(\mathbf{x}) = \frac{\rho^3}{30(1-v_0)} \times \begin{bmatrix} \left(3\rho^2 + 10v_0 - 5\right)\delta_{ij}\delta_{kl} + 15\left(1-\rho^2\right)\delta_{ij}n_k n_l \\ +\left(3\rho^2 - 10v_0 + 5\right)\left(\delta_{ik}\delta_{jl} + \delta_{il}\delta_{jk}\right) \\ +15\left(1 - 2v_0 - \rho^2\right)\delta_{kl}n_i n_j + 15\left(7\rho^2 - 5\right)n_i n_j n_k n_l \\ +15\left(v_0 - \rho^2\right)\left(\delta_{ik}n_j n_l + \delta_{il}n_j n_k + \delta_{jk}n_i n_l + \delta_{jl}n_i n_k\right) \end{bmatrix}, \tag{18}$$

where v_0 is the Poisson's ratio of the matrix and $\rho = a/r$, in which a is the radius of the sphere, $r = \sqrt{x_i x_i}$, and $n_i = x_i/r$.

For simplicity, let us consider that all particles are uniformly randomly distributed in the composites. Therefore, $P^{(\beta)}(\mathbf{x}')$ can be assumed to be $N^{(\beta)}/V$ ($\beta = 1, 2, 3, 4$), where $N^{(\beta)}$ is the total number of β-phase particles uniformly dispersed in volume V of RVE. After a series of lengthy but straightforward derivations, we arrive at the following ensemble-averaged $\langle H \rangle_m$ expression:

$$\langle H \rangle_m = \boldsymbol{\sigma}_0 : \mathbf{T} : \boldsymbol{\sigma}_0, \tag{19}$$

where the components of the fourth-rank tensor $\mathbf{T}$ for spherical particles take the form

$$T_{ijkl} = T_{IK}^{(1)}\delta_{ij}\delta_{kl} + T_{IJ}^{(2)}\left(\delta_{ik}\delta_{jl} + \delta_{il}\delta_{jk}\right) \tag{20}$$

with

$$T_{IK}^{(1)} = -\frac{1}{3} + \frac{2}{675(1-v_0)^2} \times \begin{bmatrix} (65v_0^2 - 50v_0 + 2)\sum_{\beta=1}^{4}\frac{\phi^{(\beta)}}{B_{II}^{(\beta)}B_{KK}^{(\beta)}} \\ -75(1-2v_0)^2\sum_{\beta=1}^{4}\frac{\phi^{(\beta)}\left(\Gamma_{II}^{(\beta)} + \Gamma_{KK}^{(\beta)}\right)}{B_{II}^{(\beta)}B_{KK}^{(\beta)}} \\ +225(1-2v_0)^2\sum_{\beta=1}^{4}\frac{\phi^{(\beta)}\Gamma_{II}^{(\beta)}\Gamma_{KK}^{(\beta)}}{B_{II}^{(\beta)}B_{KK}^{(\beta)}} \end{bmatrix},$$

$$T_{IJ}^{(2)} = \frac{1}{2} + \frac{(35v_0^2 - 50v_0 + 23)}{225(1-v_0)^2}\sum_{\beta=1}^{4}\frac{\phi^{(\beta)}}{B_{IJ}^{(\beta)}B_{IJ}^{(\beta)}}. \tag{21}$$

Here, $\phi^{(\beta)}$ denotes the volume fraction of the β-phase particles. Other parameters in the above equation are rendered as

$$B_{IJ}^{(\beta)} = 2\left(V_{IJ} + N_{IJ}^{(\beta)}\right), \quad \beta = 1, 2, 3, 4, \tag{22}$$

$$\begin{Bmatrix} \Gamma_{I1}^{(\beta)} \\ \Gamma_{I2}^{(\beta)} \\ \Gamma_{I3}^{(\beta)} \end{Bmatrix} = \begin{Bmatrix} U_{11} + W_{11} & U_{21} + M_{21}^{(\beta)} & U_{31} + M_{31}^{(\beta)} \\ U_{12} + M_{12}^{(\beta)} & U_{22} + W_{22} & U_{32} + M_{32}^{(\beta)} \\ U_{13} + M_{13}^{(\beta)} & U_{23} + M_{23}^{(\beta)} & U_{33} + W_{33} \end{Bmatrix}^{-1} \begin{Bmatrix} U_{I1} + M_{I1}^{(\eta)} \\ U_{I2} + M_{I2}^{(\eta)} \\ U_{I3} + M_{I3}^{(\eta)} \end{Bmatrix},$$

with

$$U_{11} = \frac{2}{3} - \frac{4}{3}v_0, \quad U_{12} = U_{13} = U_{21} = U_{31} = \frac{4}{3}v_0 - \frac{2}{3},$$

$$U_{22} = U_{33} = 3 - \frac{4}{3}v_0, \quad U_{23} = U_{32} = \frac{4}{3}v_0 - \frac{1}{6},$$

$$V_{11} = V_{12} = V_{21} = V_{13} = V_{31} = \frac{2}{3} - \frac{4}{3}v_0,$$

$$V_{22} = V_{23} = V_{32} = V_{33} = \frac{7}{6} - \frac{4}{3}v_0,$$

$$M_{IJ}^{(\beta)} = \frac{\lambda^{(0)}(1 - D_{IK}^{(\beta)}\delta_{kk}) - 2\mu^{(0)}D_{IJ}^{(\beta)}}{2(\mu_{II}^{(\beta)} - \mu^{(0)})},$$

$$N_{IJ}^{(\beta)} = \frac{\mu^{(0)}}{2(\mu_{IJ}^{(\beta)} - \mu^{(0)})},$$

$$\begin{Bmatrix} D_{I1}^{(\beta)} \\ D_{I2}^{(\beta)} \\ D_{I3}^{(\beta)} \end{Bmatrix} = \begin{bmatrix} X_{11} & \lambda_{12}^{(\beta)} - \lambda^{(0)} & \lambda_{13}^{(\beta)} - \lambda^{(0)} \\ \lambda_{12}^{(\beta)} - \lambda^{(0)} & X_{22} & \lambda_{23}^{(\beta)} - \lambda^{(0)} \\ \lambda_{13}^{(\beta)} - \lambda^{(0)} & \lambda_{23}^{(\beta)} - \lambda^{(0)} & X_{33} \end{bmatrix}^{-1} \begin{Bmatrix} \lambda_{I1}^{(2)} - \lambda^{(0)} \\ \lambda_{I2}^{(2)} - \lambda^{(0)} \\ \lambda_{I3}^{(2)} - \lambda^{(0)} \end{Bmatrix} \tag{23}$$

and

$$W_{II} = M_{II}^{(\beta)} + 2N_{II}^{(\beta)},$$

$$X_{II} = \lambda_{II}^{(\beta)} - \lambda^{(0)} + 2(\mu_{II}^{(\beta)} - \mu^{(0)}), \quad I = 1, 2, 3. \tag{24}$$

The general relationship between the applied far-field stress $\bar{\boldsymbol{\sigma}}_{\mathbf{0}}$ and the macroscopic (ensemble-volume averaged) stress $\bar{\boldsymbol{\sigma}}$ takes the form [19]

$$\boldsymbol{\sigma}_0 = \mathbf{P} : \bar{\boldsymbol{\sigma}}, \tag{25}$$

where the fourth-rank tensor $\mathbf{P}$ reads

$$\mathbf{P} = \{\mathbf{C}^{(0)} \cdot [\mathbf{I} + (\mathbf{I} - \mathbf{S}) \cdot \mathbf{Y}] \cdot \mathbf{C}^{(0)^{-1}}\}^{-1} \tag{26}$$

with

$$\mathbf{Y} = \sum_{\beta=1}^{4} \phi^{(\beta)}[\mathbf{S} + (\mathbf{C}^{(\beta)} - \mathbf{C}^{(0)})^{-1} \cdot \mathbf{C}^{(0)}]^{-1}, \tag{27}$$

where $\mathbf{S}$ is the Eshelby's tensor given in [13] for spherical particles. The combination of Eqs. (19) and (25) leads to an alternative expression of the ensemble-averaged square of the current stress norm as

$$\langle H \rangle_m = \bar{\boldsymbol{\sigma}} : \bar{\mathbf{T}} : \bar{\boldsymbol{\sigma}}, \tag{28}$$

where the fourth-rank tensor reads $\bar{\mathbf{T}} = \mathbf{P}^{\mathbf{T}} \cdot \mathbf{T} \cdot \mathbf{P}$. It is observed from the above equation that $\langle H \rangle_m$ can be reduced to the corresponding equation in [17] if no particle debonding occurs in the composites (i.e., $\phi^{(1)} > 0$ and $\phi^{(\beta)} = 0, \beta = 2, 3, 4$). Furthermore, Eq. (28) will recover the classical J_2-invariant for the matrix-only material (i.e., $\phi^{(\beta)} = 0$, $\beta = 1, 2, 3, 4$).

4 Composite constitutive modeling

For the small deformation theory, the total macroscopic strain $\bar{\boldsymbol{\varepsilon}}$ consists of two parts:

$$\bar{\boldsymbol{\varepsilon}} = \bar{\boldsymbol{\varepsilon}}^{\mathrm{e}} + \bar{\boldsymbol{\varepsilon}}^{\mathrm{p}}, \tag{29}$$

where $\bar{\boldsymbol{\varepsilon}}^{\mathrm{e}}$ denotes the overall elastic strain, and $\bar{\boldsymbol{\varepsilon}}^{p}$ represents the overall plastic strain of the composites. The relationship between the macroscopic stress $\bar{\boldsymbol{\sigma}}$ and macroscopic elastic strain $\bar{\boldsymbol{\varepsilon}}^{e}$ reads

$$\bar{\boldsymbol{\sigma}} = \bar{\mathbf{C}} : \bar{\boldsymbol{\varepsilon}}^{\mathrm{e}}, \tag{30}$$

in which the effective elastic stiffness of composites can be determined as [19]

$$\bar{\mathbf{C}} = \mathbf{C}^{(0)} \cdot [\mathbf{I} + (\mathbf{Y}^{-1} - \mathbf{S})^{-1}]. \tag{31}$$

In the above equation, $\mathbf{Y}$ has previously been defined in Eq. (27). The plastic flow of composites is postulated to be associative for simplicity. The macroscopic plastic strain rate for PRMMCs thus takes the form

$$\dot{\bar{\boldsymbol{\varepsilon}}}^{p} = \dot{\lambda} \frac{\partial \bar{F}}{\partial \bar{\boldsymbol{\sigma}}}, \tag{32}$$

where $\dot{\lambda}$ is the plastic consistency parameter. Moreover, $\bar{F}$ is the overall yield function of composites (cf. Eq. (14)). The simple isotropic power-law hardening function $K(\bar{e}^{p})$ is proposed as

$$K(\bar{e}^{p}) = \sqrt{\frac{2}{3}}[\sigma_y + h(\bar{e}^{p})^{q}]. \tag{33}$$

Here, σ_y denotes the initial yield stress of matrix material, and h and q signify the linear and exponential isotropic hardening parameters.

The foregoing characterization together with the Kuhn-Tucker conditions

$$\dot{\lambda} \geq 0, \quad \bar{F} \leq 0, \quad \dot{\lambda}\bar{F} = 0, \quad \dot{\lambda}\dot{\bar{F}} = 0 \tag{34}$$

then constitutes an effective elastoplastic-damage constitutive formulation for particle-reinforced metal matrix composites with a progressive, partial interfacial debonding process. The proposed composite framework as formulated in Eqs. (29)–(34) is based on the micromechanics approach, the ensemble-averaging homogenization procedures, and the statistical distribution method. The proposed formulation offers a potentially viable framework to estimate the overall elastoplastic-damage stress-strain responses of the metal matrix composites.

5 Numerical examples

5.1 Uniaxial tensile loading

The uniaxial stress-strain curves are often referred to as important indicators of mechanical behaviors of composite materials. In order to illustrate the proposed micromechanics-based model, let us first consider the uniaxial tension loading. In this case, the components of the macroscopic stress $\bar{\boldsymbol{\sigma}}$ can be expressed as $\bar{\sigma}_{11} > 0$ and $\bar{\sigma}_{ij} = 0$ for all other stress components. Unless noted otherwise, during the subsequent numerical simulations, the selected composite system signifies the SiC particle reinforced aluminum matrix composite. The Young's moduli and Poisson's ratios of SiC particles and the aluminum matrix are taken as $E_p = 450$ GPa, $E_m = 70$ GPa, $v_p = 0.2$ and $v_m = 0.3$, where the subscripts p and m represent the particles and the matrix, respectively. The Weibull's parameter is selected as $M = 5$. The yield strength is taken as $\sigma_y = 300$ MPa and the hardening parameters are assumed to be $h = 1.0$ GPa and $q = 0.5$, respectively. Numerical simulations on the uniaxial elastoplastic-damage stress-strain behaviors of PRMMCs are displayed in Fig. 5. Clearly, the effective stress-strain responses for a 15% volume fraction of spherical particles with progressive interfacial debonding lie between those of the porous material (the lower bound) and the composite material without debonding (the upper bound). The interfacial bonding strength plays an

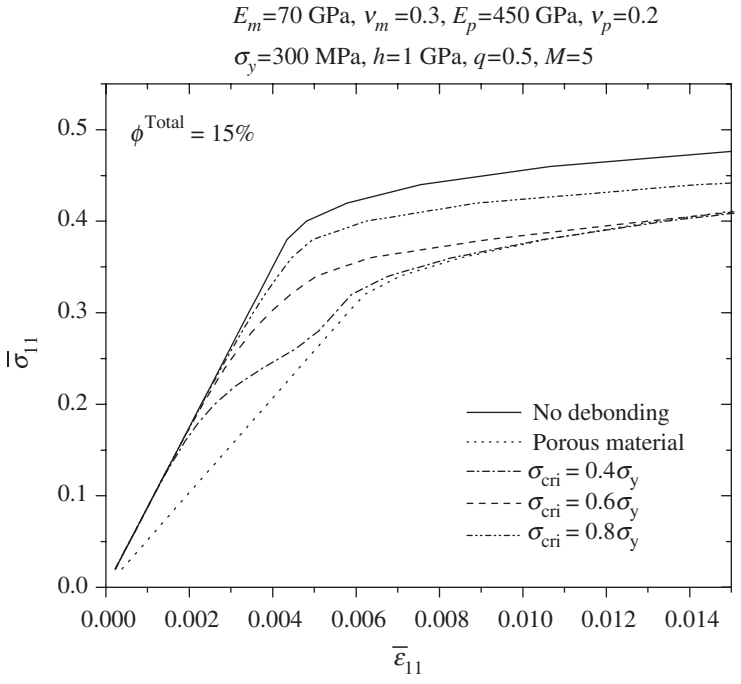

Fig. 5. The overall stress-strain curves of PRMMCs with progressive interfacial debonding

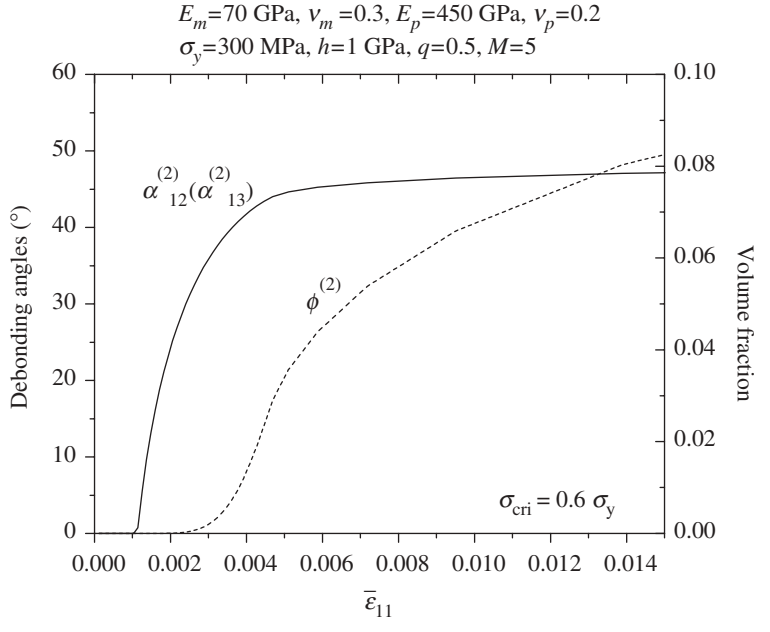

Fig. 6. The evolution of debonding angles (solid line) and volume fraction (dashed line) with the increased overall strain in uniaxial loading case

important role in the interfacial debonding process, and has significant effects on the overall elastoplastic-damage behaviors of the composites, see Fig. 5. Specifically, less strain hardening can be clearly observed for composites with lower interfacial bonding strengths. For

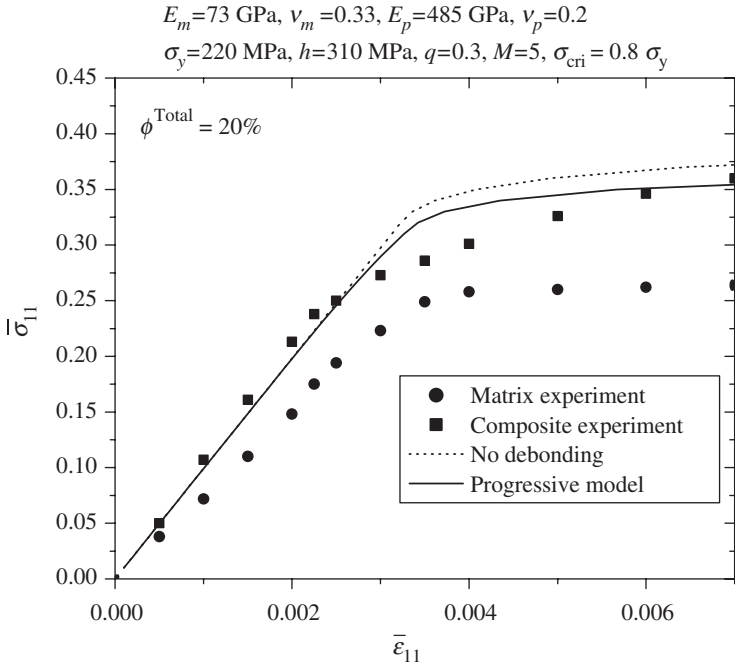

Fig. 7. The comparison between the prediction of current model and the experimental result [20]

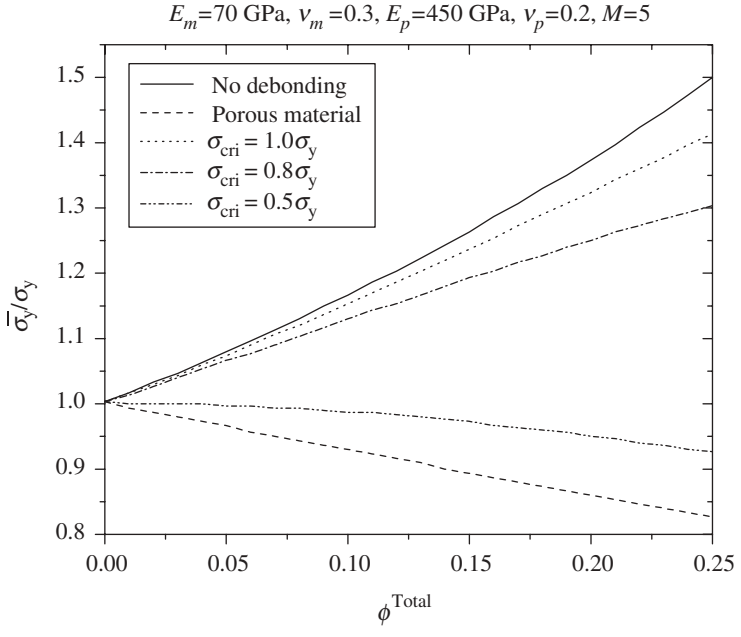

Fig. 8. Initial yield stress vs volume fraction of particles for PRMMCs under uniaxial loading

example, with a very low bonding strength (i.e., $\sigma_{cri} = 0.4\ \sigma_y$ in Fig. 5), the interfacial debonding occurs even before the composite reaches its overall yield point and therefore a softening portion can be observed.

Under the uniaxial loading condition, the first local principal stress is tensile and the other two local principal stresses are compressive with the same magnitudes. Therefore, only one debonding mode – debonding along the loading direction – will occur. In Fig. 6, the solid line shows the debonding-angle progression as a function of the overall strain history. Because of the equality of the second and third local principal stresses, the debonding angles $\alpha_{12}^{(2)}$ and $\alpha_{13}^{(2)}$ are equal to each other. From this figure, it is observed that the debonding angle increases rapidly at the beginning stage, and then becomes saturated as the overall deformation increases, implying that it is increasingly more difficult to further debond due to the compressive principal stresses in the second and third principal directions. The dashed line in Fig. 6 displays the evolution process of the damaged volume fraction of particles. Since there is only one debonding mode (mode 2), $\phi^{(2)}$ increases during the entire loading process while the other damaged volume fractions ($\phi^{(3)}$ and $\phi^{(4)}$) remain zero.

Figure 7 exhibits the comparison between our analytical model predictions and the experimental results of particulate-reinforced SiC/Al5456 composites reported by Papazian and Adler [20]. With the introduction of progressive interfacial debonding, our current model obtains a better prediction than the non-debonding model. The effects of debonding on the overall initial yield strengths of the composites are rendered in Fig. 8. When the particle volume fraction is zero, there are no reinforcements in the composite and therefore it becomes a matrix-only material. The overall yield strengths of the composites increase with increasing volume fractions of particles without considering debonding, which reflects the enhancing hardening influence of the existence of reinforcing particles. By contrast, for porous materials with voids, a higher volume fraction of voids leads to a decrease of the overall initial yield strength. With higher particle concentrations in the composites, the interfacial debonding mechanism creates

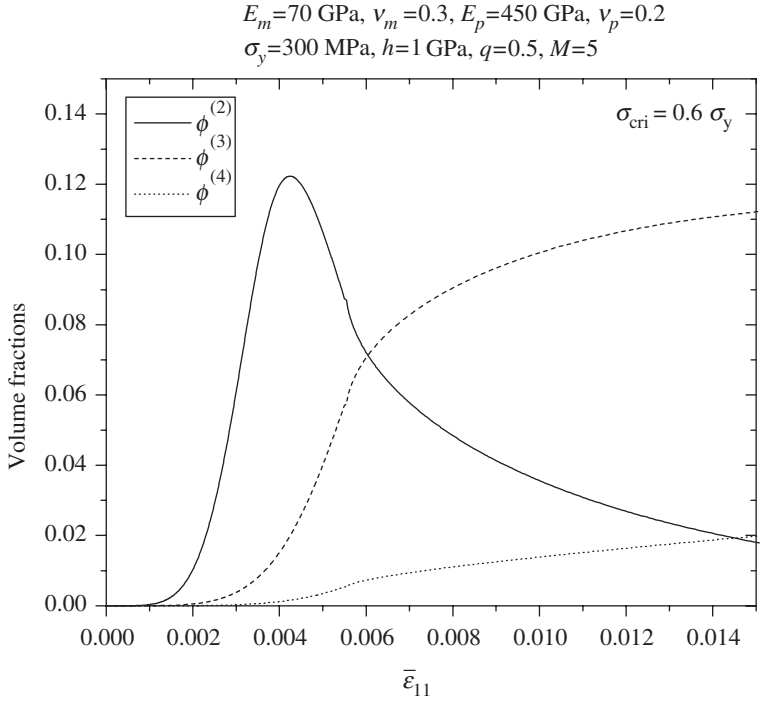

Fig. 9. The evolution of volume fractions with the increased overall strain under triaxial loading condition

more pronounced effects on the overall initial yield strengths of the composites. Moreover, as the bonding strength becomes weaker, particle debonding occurs in an early loading stage; and as the overall initial yield takes place, there are already many void-like particles in the composites. As a consequence, the overall initial yield strengths of the weak-interface composites go even lower than the matrix-only material, and the voids-prone composites behave like porous materials.

5.2 Triaxial tensile loading

Under the uniaxial loading condition, only one debonding mode is active since only the first local principal stress is tensile. To investigate the transformation between different debonding modes, the composite is subjected to the triaxial loading case, in which $\bar{\sigma}_{11} > 0$, $\bar{\sigma}_{22} = 0.6\bar{\sigma}_{11}$ and $\bar{\sigma}_{33} = 0.4\bar{\sigma}_{11}$. Figure 9 shows the evolution and transformation of the damage volume fractions. With the increase of the overall external loading, the first local principal stress reaches the critical strength first and activates the second debonding mode (one-dimensional debonding). Further increasing the external loading, the third debonding mode (two-dimensional debonding) becomes active when the second local principal stress reaches the critical strength. At the beginning stage, the number of newly formed mode-2 particles from the perfectly bonded (mode-1) particles is larger than the amount of mode-2 particles that evolve into mode-3 and mode-4 ones. Therefore, both $\phi^{(2)}$ and $\phi^{(3)}$ increase with the increasing external loading until a specific point where more mode-2 particles become mode-3 and mode-4 while $\phi^{(2)}$ begins to decrease. Finally, all the local principal stresses go beyond the critical strength, and all four modes of particles exist in the matrix simultaneously. The progression of debonding angles is shown in Fig. 10. Comparing with the uniaxial loading case, the debonding process develops more rapidly and the debonding angles reach the maximum value (90°) finally due to the tensile

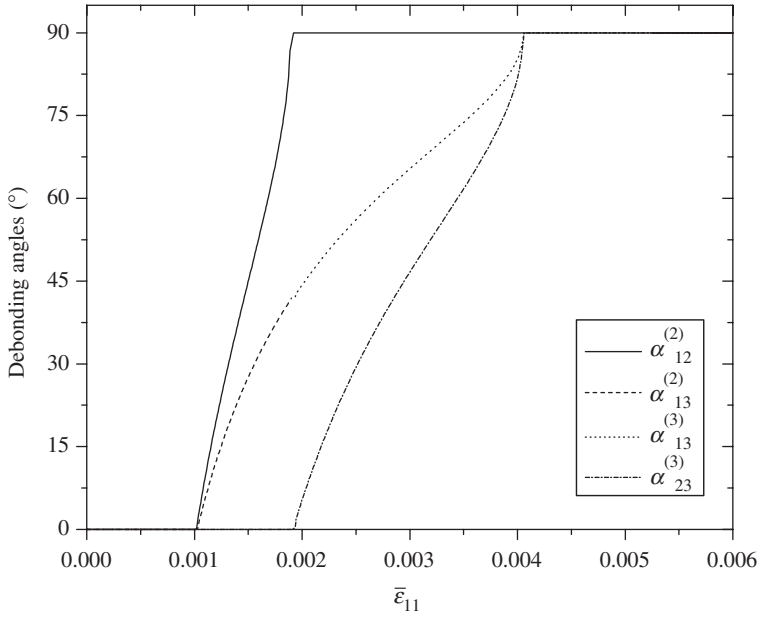

Fig. 10 The progress of debonding angles with the increased overall strain under triaxial loading condition

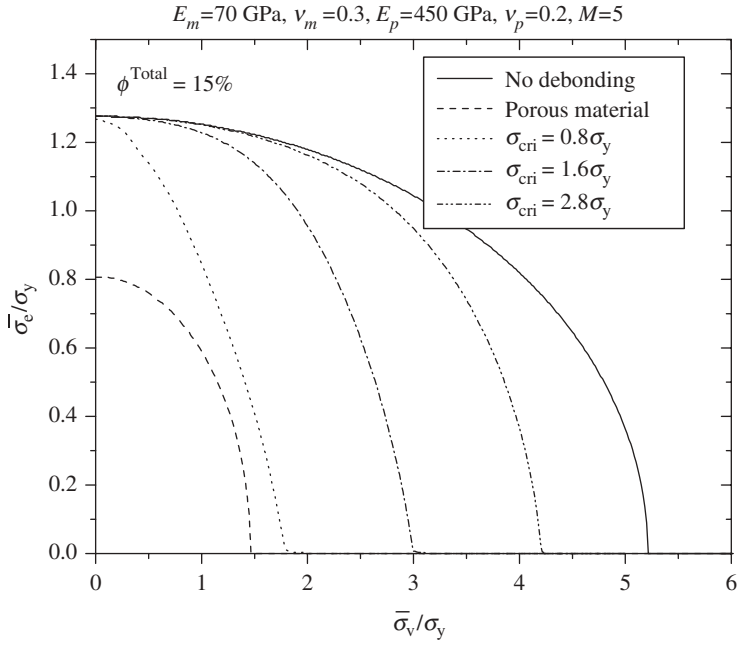

Fig. 11. Effects of bonding strengths on the overall yield surfaces for PRMMCs

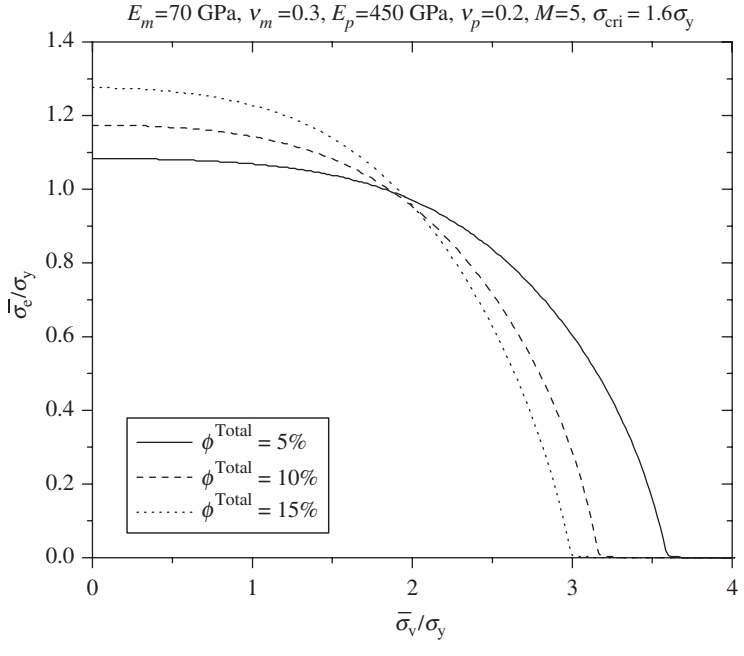

Fig. 12. Effects of volume fractions on the overall yield surfaces for PRMMCs

state of the principal stresses in all directions. When the second principal stress reaches the critical strength, the debonding angle $\alpha_{12}^{(2)}$ becomes 90° indicting a total debonding between the local x_1- and x_2-directions. Therefore, the two-dimensional debonding mode is activated (referring to $\phi^{(3)}$ in Fig. 9). The debonding angle in x_1x_3-direction ($\alpha_{13}^{(2)}$) keeps developing under

the two-dimensional debonding mode ($\alpha_{13}^{(3)}$). Once all the debonding angles progress to 90, the total debonding mode (mode-4) is achieved (referring to $\phi^{(4)}$ in Fig. 9).

To investigate the effects of interfacial particle debonding on the overall initial yield surfaces, axisymmetric (biaxial) loading cases are considered here. In this loading case, $\bar{\sigma}_{11} > 0$, $\bar{\sigma}_{22} = \bar{\sigma}_{33} > 0$ and $\bar{\sigma}_{12} = \bar{\sigma}_{13} = \bar{\sigma}_{23} = 0$. The initial effective yield surfaces are presented in terms of the normalized volumetric and effective stresses in Figs. 11 and 12. Specifically, the volumetric and effective stresses can be easily obtained from their basic definitions under the axisymmetric condition as $\bar{\sigma}_v = (\bar{\sigma}_{11} + 2\bar{\sigma}_{22})/3$ and $\bar{\sigma}_e = \bar{\sigma}_{11} - \bar{\sigma}_{22}$, respectively. Figure 11 shows that the overall initial yielding of the composites is not of the von Mises type, even though the particles are spherical in shape and randomly distributed. The effect of interfacial bonding strength is significant on the normalized volumetric yield stress, whereas considerably less influence is observed on the normalized effective yield stress. With decreasing bonding strength, early debonding occurs in the composite and causes the degradation of the initial plastic yielding point for the volumetric stress. On the other hand, for a constant (specified) bonding strength, the effects of particle volume fraction on the overall initial yield surface in the volumetric and effective stress space are exhibited in Fig. 12. In particular, decreasing particle volume fraction leads to an increase in the normalized volumetric yield stress yet a decrease in the normalized effective yield stress. This unique feature clearly illustrates that the non–von-Mises type of composite yielding is mainly caused by the existence of particles. As the volume fraction of particles reduces to zero, the matrix-only material recovers the von Mises plastic yielding, as expected.

6 Concluding remarks

Emanating from the eigenstrain concept of micromechanics and homogenization, the ensemble-averaged elastoplastic-damage constitutive equations are derived for PRMMCs with progressive partial interfacial debonding evolution. The debonding areas are represented by the corresponding debonding angles. Four different debonding modes are considered and the corresponding equivalent orthotropic stiffness tensors are constructed systematically. The proposed formulation is subsequently applied to the uniaxial and the axisymmetric (biaxial) tensile loading conditions to illustrate the potential capabilities of the present framework. Comparisons between the model predictions and the available experimental data are also conducted. The effects of the partial particle debonding on the overall initial yield stresses and yield surfaces are discussed in detail. It is noted that the proposed elastoplastic-damage formulation is amenable to generalization to handle multi-axial loading conditions. Further research is warranted to extend the current framework to accommodate the spheroidal and other particle shapes. In addition to the stress-based particle-debonding criterion, the strain-based, the energy-based or the mixed matrix-particle interfacial debonding criteria can be taken into consideration for different composite materials.

Acknowledgements

This work was sponsored by the NASA Iowa Space Grant Consortium, the National Science Foundation (CMS-0084629), the Faculty Research Grant of the UCLA Academic Senate (4-592565-19914), and Bellagio Engineering. These supports are gratefully acknowledged.

References

[1] Clyne, T. W., Withers, P. J.: An introduction to metal matrix composites. Cambridge: Cambridge University Press 1993.

[2] Suresh, S., Mortensen, A., Needleman, A.: Fundamentals of metal-matrix composites. Boston, MA: Butterworth-Heinemann 1993.

[3] Jasiuk, I., Tong, Y.: The effect of interface on the elastic stiffness of composites. Mechanics of composite materials and structures. Proc. 3rd Joint ASCE/ASME Conf. (Reddy, J. N., Teply, J. L., eds.), pp. 49–54 (1989).

[4] Pagano, N. J., Tandon, G. P.: Modeling of imperfect bonding in fiber reinforced brittle matrix composites. Mech. Mater. **9**, 49–64 (1990).

[5] Qu, J.: The effect of slightly weakened interfaces on the overall elastic properties of composite materials. Mech. Mater. **14**, 269–281 (1993).

[6] Sangani, A. S., Mo, G.: Elastic interactions in particulate composites with perfect as well as imperfect interfaces. J. Mech. Phys. Solids **45**, 2001–2031 (1997).

[7] Zhao, Y. H., Weng, G. J.: Transversely isotropic moduli of two partially debonded composites. Int. J. Solids Struct. **34**, 493–507 (1997).

[8] Wong, F. C., Ait-Kadi, A.: Analysis of particulate composite behavior based on non-linear elasticity and modulus degradation theory. J. Mater. Sci. **32**, 5019–5034 (1997).

[9] Sun, L. Z., Ju, J. W., Liu, H. T.: Elastoplastic modeling of metal matrix composites with evolutionary particle debonding. Mech. Mater. **35**, 559–569 (2003).

[10] Eshelby, J. D.: The determination of the elastic field of an ellipsoidal inclusion and related problems. Proc. Roy. Soc. Lon. **A241**, 376–396 (1957).

[11] Eshelby, J. D.: The elastic field outside an ellipsoidal inclusion. Proc. R. Soc. Lon. **A252**, 561–569 (1959).

[12] Mura, T.: Micromechanics of defects in solids, 2nd ed. Amsterdam: Kluwer Academic Publishers 1987.

[13] Liu, H. T., Sun, L. Z., Ju, J. W.: An interfacial debonding model for particle-reinforced composites. Int. J. Damage Mech. **14**, 163–185 (2004).

[14] Zhao, Y. H., Weng, G. J.: The effect of debonding angle on the reduction of effective moduli of particle and fiber-reinforced composites. J. Appl. Mech. **69**, 292–302 (2002).

[15] Tohgo, K., Weng, G. J.: A progressive damage mechanics in particle-reinforced metal-matrix composites under high triaxial tension. J. Eng. Mater-T ASME **116**, 414–420 (1994).

[16] Nemat-Nasser, S., Hori, M.: Micromechanics: Overall properties of heterogeneous materials, 2nd ed. Amsterdam: North-Holland 1999.

[17] Ju, J. W., Sun, L. Z.: Effective elastoplastic behavior of metal matrix composites containing randomly located aligned spheroidal inhomogeneities, part I: Micromechanics-based formulation. Int. J. Solids Struct. **38**, 183–201 (2001).

[18] Ju, J. W., Sun, L. Z.: A novel formulation for exterior-point Eshelby's tensor of an ellipsoidal inclusion. J. Appl. Mech. **66**, 570–574 (1999).

[19] Ju, J. W., Chen, T. M.: Micromechanics and effective moduli of elastic composites containing randomly dispersed ellipsoidal inhomogeneities. Acta Mech. **103**, 103–121 (1994).

[20] Papazian, J. M., Adler, P. N.: Tensile properties of short fiber-reinforced SiC/Al composites, part I: Effect of matrix precipitates. Metall. Trans. **A21**, 401–410 (1990).

Authors' addresses: H. T. Liu and L. Z. Sun, Department of Civil and Environmental Engineering and Center for Computer-aided Design, The University of Iowa, Iowa City, IA 52242-1527, U.S.A. (E-mail: lizhi-sun@uiowa.edu); J. W. Ju, Department of Civil and Environmental Engineering, University of California, Los Angeles, CA 90095-1593, U.S.A.